

¹ A Mathematical Study of the Efficacy of Possible Negative Feedback
² Pathways Involved in Neuronal Polarization

³ Fan Bai¹, Richard Bertram^{1,2,3}, and Bhargav R. Karamched ^{*1,2,3}

⁴ ¹Department of Mathematics, Florida State University, Tallahassee FL 32306, United States

⁵ ²Program in Molecular Biophysics, Florida State University, Tallahassee FL 32306, United States

⁶ ³Program in Neuroscience, Florida State University, Tallahassee FL 32306, United States

*Corresponding author: bkaramched@fsu.edu

7 **Highlights:**

8 1. Bistability and random excitation amplitude reduction are minimum requirements for neuronal polarization.

9 2. There exists an optimal neurite count, excitation amplitude, and excitation rate that best maintain polarization.

10 3. Our findings are consistent with previously published, more detailed models which are catered to specific exper-

11 imental observations.

12 Abstract

13 Neuronal polarization, a process wherein nascent neurons develop a single long axon and multiple short dendrites,
14 can occur within *in vitro* cell cultures without environmental cues. This is an apparently random process in which
15 one of several short processes, called neurites, grows to become long, while the others remain short. In this study,
16 we propose a minimum model for neurite growth, which involves bistability and random excitations reflecting actin
17 waves. Positive feedback is needed to produce the bistability, while negative feedback is required to ensure that no
18 more than one neurite wins the winner-takes-all contest. By applying the negative feedback to different aspects of the
19 neurite growth process, we demonstrate that targeting the negative feedback to the excitation amplitude results in
20 the most persistent polarization. Also, we demonstrate that there are optimal ranges of values for the neurite count,
21 and for the excitation rate and amplitude that best maintain the polarization. Finally, we show that a previously
22 published model for neuronal polarization based on competition for limited resources shares key features with our
23 best-performing minimal model: bistability and negative feedback targeted to the size of random excitations.

24 Keywords: Neuronal polarization, bistability, negative feedback, stochastic dynamical system.

25 Introduction

26 A nervous system is composed of interconnected neurons, each of which has multiple short dendrites that receive
27 signals from upstream neurons and a single long axon that transmits signals to downstream neurons. Early in
28 development, however, a neuron has multiple short neurites of similar lengths that extend and retract repeatedly
29 and apparently randomly (coined by [1] as Stage 2). These neurites later differentiate into dendrites and a single
30 axon (Fig. 1). The symmetry-breaking process by which a single axon emerges from the neurites (Stage 3) is referred
31 to as *neuronal polarization*. Surprisingly, this process does not require release of growth factors from target cells, as
32 neuronal polarization has been shown to occur within *in vitro* hippocampal neuron cell cultures in which there are
33 no growth factor gradients guiding the selection process [1, 2]. The symmetry breaking appears to be random, and in
34 experiments where the initial axon was cleaved off, a new one emerged from one of the other neurites [3]. Subsequent
35 experimental manipulations demonstrated that it was possible for any neurite to become the winning neurite in the
36 winner-takes-all contest [4, 5]. It has been shown that even in the *in vivo* setting where growth factor gradients are
37 present, the developing neurons go through these stages, lasting about a day, characterized by growth and retraction
38 of neurites with a subsequent symmetry breaking event [6, 7]. In this case, growth factor gradients influence the
39 selection process, and indeed the random growth and retraction of neurites is thought to be a way for the neurites to
40 explore the environment to seek out the growth factors (called *neurotrophins*). Nonetheless, even *in vivo* there is a
41 winner-takes-all process that takes place, with bias provided by neurotrophin gradients.

42 There have been many studies aimed at understanding the biophysical mechanism of the neuronal polarization
43 process [4, 8–13]. Several potential mechanisms have been identified, and it is clear that the process involves positive
44 feedback signals to promote the growth of the axon as well as negative feedback signals to prevent the emergence of
45 a second axon [10, 13–16]. In this article, we focus on the polarization process that occurs *in vitro*, without external
46 neurotrophin gradients, using a minimal model for the winner-take-all selection process that incorporates positive
47 feedback and explore the efficacy of several different negative feedback mechanism in generating persistent neuronal
48 polarization.

49 The model is constructed based on the hypothesis that the dynamics underlying neurite growth and retraction are
50 such that the system is bistable. That is, each neurite has two stable equilibria, short and long. The bistability is a

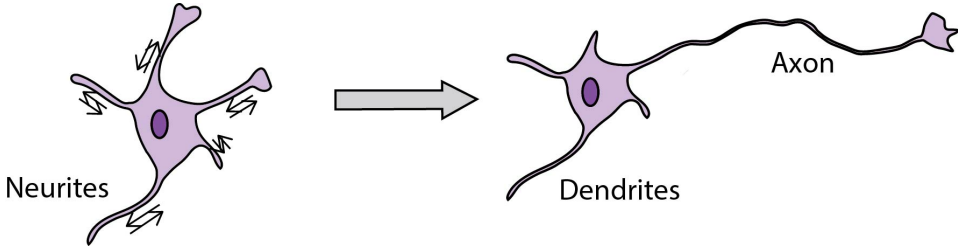


Figure 1: Neuronal polarization. A nascent neuron (stage 2) has several short neurites that extend and retract repeatedly and randomly (left). Later, during stage 3, one of the neurites develops into an axon while others become dendrites (right).

51 product of the positive feedback. A second hypothesis is that the selection process is truly random, so no neurite is
 52 biased towards winning the competition to become an axon. We then explore three mechanisms of negative feedback.
 53 One of these involves the retraction rate that is common to all neurites. The others involve a stochastic term that
 54 reflects randomly-timed and uniformly distributed actin waves which are known to be key to neurite elongation; each
 55 actin wave provides growth spurts by locally increasing the neurite volume to allow for microtubule polymerization
 56 [12, 17, 18]. We consider the effects of making neurite retraction, actin wave magnitude, and actin wave frequency
 57 dependent on the combined length of the neurites such that increased length increases the retraction rate, or decreases
 58 the actin wave magnitude or frequency. In all cases, the negative feedback is unbiased.

59 The results demonstrate that targeting the negative feedback to the stochastic growth magnitude (i.e., the actin
 60 wave term) results in the most persistent polarized system. They also demonstrate that having more than 2 neurites,
 61 but less than some upper bound, is optimal for achieving and maintaining neuronal polarization. This is consistent with
 62 the finding that most nascent neurons have between 2 and 10 neurites [2]. One model for neuronal polarization is based
 63 on competition for limited resources, including growth factor [16]. In the last section of Results, we demonstrate that
 64 a simplified model based on this limited-resource model contains the two elements that we find to be most successful
 65 at achieving persistent polarization: bistability and length-dependent reduction in the amplitude of actin-wave-driven
 66 stochastic excitation .

67 The Minimal Model

68 We consider a small population of R neurites, each with length L_i , $i = 1, 2, \dots, R$. The basic model contains a term
 69 for positive feedback, a retraction term, and a stochastic term reflecting randomly-timed actin waves. The negative
 70 feedback is included later. The basic model is:

$$\frac{dL_i}{dt} = g \frac{L_i^2}{L_i^2 + K^2} - rL_i + \sum_n A\delta(t - t_n^{(i)}(\lambda)), \quad i = 1, 2, \dots, R. \quad (1)$$

71 The first term reflects positive feedback through intracellular signaling [8, 10, 11, 13, 15, 19], length-dependent diffusion
 72 of polarity effectors [16, 20, 21], and stabilization of microtubules [22, 23]. Positive feedback is an essential ingredient
 73 of bistability [24]. The second term provides a constant rate of neurite retraction, reflecting the retraction that occurs
 74 in all neurites between the arrival of actin waves [25]. The last term includes a sum of delta functions that describes
 75 sudden neurite elongation due to actin waves [25–27]. Each wave induces a jump in length of size A . The term $t_n^{(i)}(\lambda)$
 76 is the time when the tip of the i th neurite receives the n th wave, which follows a Poisson process of rate λ (this is also
 77 the average number of waves generated per unit time).

78 With our minimal model, a neurite can be thought of as a particle in a double-well potential, as shown in Fig. 2A.
 79 The left potential well corresponds to the state of being a short neurite, and the right well corresponds to the state of

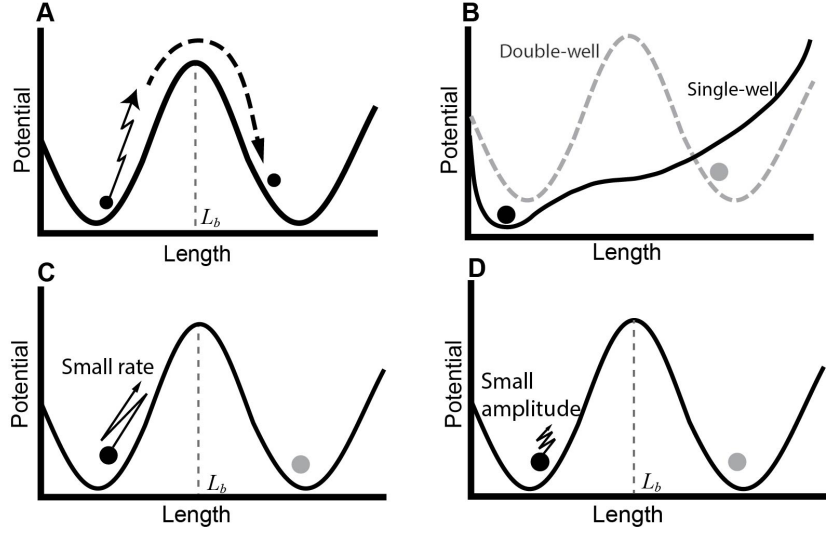


Figure 2: The bistability in the neurite growth model interpreted as a double well potential and the effects of negative feedback. (A) The double well potential shows the bistability in neuronal polarization. Due to random excitations, a particle representing a neurite may cross the potential barrier, located at position L_b . (B) The increased retraction rate due to the formation of an axon (grey dot) destroys the double well potential for a short neurite (black dot). (C) Under the excitation rate reduction, the particle falls back significantly between two excitations. (D) Under the excitation amplitude reduction, each pulse only helps the particle climb a short distance.

80 being a long neurite that will become an axon. The actin waves then provide random excitations that can drive the
 81 particle across the potential barrier at location L_b , marking the establishment of an axon. All nascent neurons have
 82 short neurites, so they begin in the left potential well.

83 Since only one neurite develops into the axon of a typical neuron, the growth of other neurites should be suppressed
 84 to avoid having multiple axons. One way to incorporate this negative feedback into the model is to have the retraction
 85 rate r increase as the neurites get longer. For simplicity, we use the following length-dependent retraction rate:

$$r = r_0 \left(1 + \alpha \sum_{i=1}^R L_i \right), \quad (2)$$

86 where r_0 is a basal retraction rate and α is a parameter that controls the degree of suppression. The retraction rate
 87 is the same for every neurite, so the suppression is unbiased. Reducing the growth rate g in an unbiased way will give
 88 qualitatively similar results. Targeting the negative feedback to the retraction rate has the effect of eliminating the
 89 upper equilibrium state for each of the short neurites (Fig. 2B). Biologically, the increased retraction rate reflects the
 90 collection of inhibitory signals in the cell body sent from the neurite tips.

91 Since actin waves drive neurite growth, negative feedback can also be implemented by suppressing the generation
 92 of the waves. In our model, this is done by reducing the excitation rate λ according to the following equation:

$$\lambda = \frac{\lambda_0}{1 + \mu \sum_{i=1}^R L_i}, \quad (3)$$

93 where λ_0 is a basal excitation rate and μ controls the degree of reduction. Again, the inhibition is unbiased because
 94 the actin waves are shared equally among neurites. Under the rate reduction, a neurite retracts significantly between
 95 two waves, so its net growth is small (Fig. 2C). A length-dependent decrease in actin wave frequency is consistent with
 96 the observation that actin waves are less frequent once an axon is formed [18]. This inhibitory mechanism was also
 97 implemented in a previous mathematical model [21, 28].

Notation	Definition	Value
g	Maximum growth rate	10
K	Half activation level	$\sqrt{21}$
r_0	Basal retraction rate	1
α	Feedback coefficient of increased retraction	0.026
λ_0	Basal excitation rate	1
μ	Feedback coefficient of reduced excitation rate	0.4
A_0	Basal excitation amplitude	1
ϕ	Feedback coefficient of reduced excitation amplitude	0.4
L_b	Location of the potential barrier	3

Table 1: List of parameters and their values used in the study of different negative feedback mechanisms.

98 Finally, we implement negative feedback by reducing the amplitude A as follows:

$$A = \frac{A_0}{1 + \phi \sum_{i=1}^R L_i}, \quad (4)$$

99 where A_0 is a basal excitation amplitude and ϕ controls the degree of reduction. In terms of the particle in a double well
100 potential, a reduced amplitude means that more excitations will be required to cross the potential barrier (Fig. 2D).
101 Biologically, actin waves carry growth factors produced at the cell body, so amplitude reduction could reflect depletion
102 of the growth factors. A similar amplitude reduction mechanism was adopted in a previous modeling study [16].

103 Persistence of Polarization with Different Forms of Negative Feedback

104 For mathematical simplicity, we consider a nascent neuron with two neurites ($R = 2$) in this section. In fact, neurons
105 with two neurites were also observed in experiments [2]. For such a neuron, we study the effect of each of the
106 three negative feedback mechanisms from three perspectives: (1) the joint probability density of the lengths, denoted
107 by $p(L_1, L_2)$, (2) the underlying deterministic phase portraits, and (3) the stochastic dynamics. To analyze the
108 probability density and stochastic dynamics, we employ two complementary methods: the generalized cell-mapping
109 method (GCM) and Monte Carlo (MC) simulations, which are explained in detail in the Appendix. The GCM allows
110 us to efficiently determine the probability density of the lengths and its long-term limit. However, when dealing with
111 neurons possessing more than two neurites, the GCM becomes computationally expensive. In such cases, the MC
112 method proves to be more efficient, particularly when the timescale is short. Additionally, the MC method unveils
113 neurite dynamics that are not captured by the probability density obtained through the GCM. Nevertheless, the MC
114 method is less effective than the GCM in analyzing the long-term behavior of the probability density.

115 We begin by considering negative feedback through a length-dependent increase in the neurite retraction rate
116 (Eq. (2)). The long-term joint probability distribution of the lengths exhibits two peaks, which indicates that the
117 system spends most of the time near these peaks (Fig. 3A). Each peak represents a state with a long neurite and a
118 short neurite, which we refer to as a *polarized state*. The formation of the peaks can be inferred from the following
119 deterministic system:

$$\frac{dL_i}{dt} = g \frac{L_i^2}{L_i^2 + K^2} - rL_i + \frac{1}{2} A\lambda, \quad i = 1, 2, \quad (5)$$

120 where the term $\frac{1}{2} A\lambda$ is the time average of the Poissonian term in Eq. (1). The factor $1/2$ accounts for the fact that the
121 total number of actin waves is divided between the two neurites. We continue to use L_i for the neurite lengths in this
122 system, though they are no longer random variables. Figure 3B shows nullclines and the vector field for Eq. (5). There
123 are seven equilibria, three of which are stable. Two correspond to the polarized state and are near the peaks of the
124 probability distribution, while one near the origin corresponds to a state in which both neurites are short. The basin

125 of attraction of the latter is small, so in the stochastic system described next trajectories leave this region quickly.

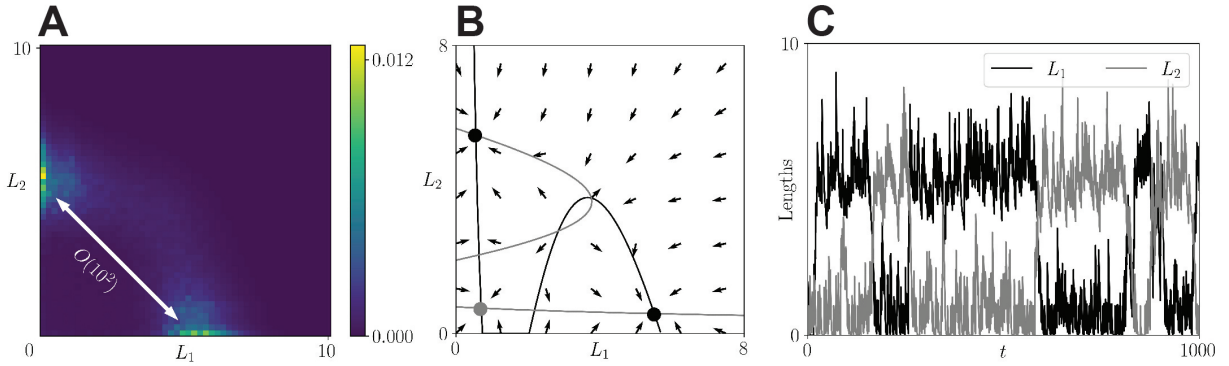


Figure 3: The dynamics of the two-neurite system when negative feedback targets the retraction rate. (A) The long-term probability density of the neurite lengths exhibits two peaks. The mean transition time between the peaks is of $O(10^2)$, which is estimated by the mean time to enter $[4, 8] \times [0, 2]$ from $(0, 6)$. (B) The phase portrait of Eq. (5) shows two stable equilibria close to the peaks of the stationary probability density, corresponding to two polarized states. The L_1 -nullclines (black) and L_2 -nullclines (grey) intersect at 5 additional locations, one of which (grey point) is a stable equilibrium. (C) Monte Carlo simulation shows frequent alternations in the lengths of neurite 1 (black) and neurite 2 (grey). To study the effect of the increased retraction alone, we set $\lambda = \lambda_0$ and $A = A_0$. Other parameter values are given in Table 1.

126 The bimodal probability density does not necessarily imply a firmly established axon. Monte Carlo simulations
 127 show that both neurite lengths alternate between two levels. That is, the system makes frequent transitions between
 128 the two polarized states (Fig. 3C). This is further indicated by the short mean transition time from one peak to the
 129 other ($O(10^2)$ time units; see Fig. 3A). Thus, a single polarized state is not maintained when the negative feedback is
 130 implemented upon the retraction rate.

131 We next explore the dynamics in which negative feedback is implemented through length-dependent reduction in
 132 the excitation rate as prescribed by Eq. (3). The joint probability density initially has two peaks at the two polarized
 133 states. As time progresses, however, the polarized peaks fade and a third peak corresponding to two long neurites
 134 gains prominence (the top right peak in Fig. 4A). The mean transition time from a polarized state to the nonpolarized
 135 state is $O(10^3)$ time units (Fig. 4A). All three states appear as stable equilibria in the deterministic system, in addition
 136 to the stable equilibrium with a small basin of attraction corresponding to two short neurites (Fig. 4B). A Monte Carlo
 137 simulation shows the early development of a polarized state, followed by a transition to a state with two long neurites
 138 at $t \approx 1000$ (Fig. 4C). These results indicate that this form of negative feedback is not effective at maintaining a
 139 persistent polarized state. Incorporating both length-dependent increased retraction rate and reduced excitation rate
 140 eliminates the two long-neurite state (Fig. 5A and B), but does not prevent flipping between polarized states (Fig. 5C).

141 Finally, we consider negative feedback implemented through a length-dependent reduction in the excitation am-
 142 plitude as prescribed by Eq. (4). Unlike the excitation rate reduction, the amplitude reduction yields a bimodal
 143 probability density that develops almost immediately (at $t = O(10)$, see Fig. 6A) and persists even at $t = 10^6$ (to
 144 be explained in the next section). A peak in which both neurites are long does not appear until much later, and
 145 the mean transition time from a polarized state to this nonpolarized state is $O(10^9)$ (Fig. 6B), which is much larger
 146 than the mean transition time when negative feedback is through rate reduction. Biologically, this means that the
 147 polarized state persists long enough that later stages of neuron development, including targeting of the nascent axon
 148 to appropriate targets via neurotrophins, can occur. Also, the system does not flip between the two polarized states, as
 149 shown with a Monte Carlo simulation (Fig. 6C). These results indicate that implementing negative feedback through
 150 a length-dependent reduction in the excitation amplitude results in persistent neuronal polarization.

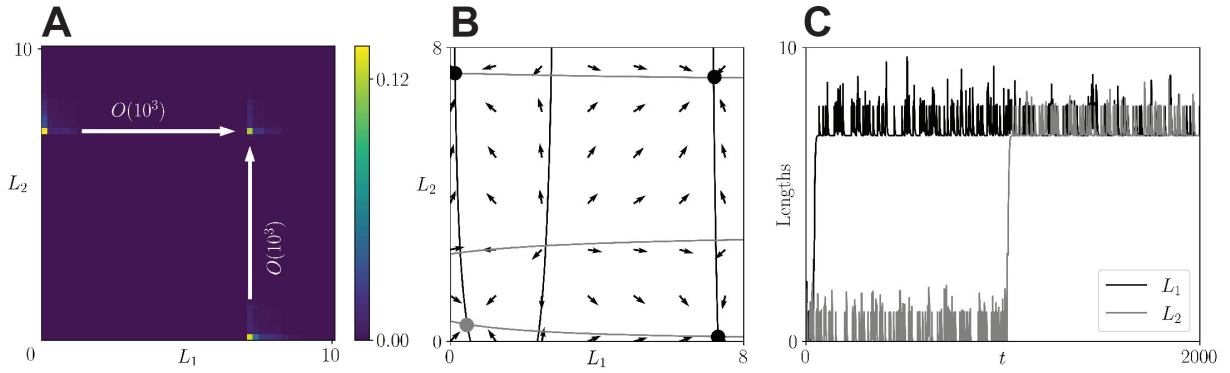


Figure 4: The dynamics of the two-neurite system with negative feedback implemented through a length-dependent reduction in the excitation rate. (A) The probability density at $t = 400$ shows peaks at the two polarized states as well as a peak in which both neurites are long. The mean transition time from a polarized state to a nonpolarized state is $O(10^3)$ time units, estimated by the mean time to reach $[6, 10] \times [6, 10]$ from $(0, 8)$. (B) The phase portrait shows two stable equilibria at polarized states (black circles), another in which both are short (grey), and another in which both are long (black). (C) A Monte Carlo simulation shows that both neurites become long at $t \approx 1000$. To study the effect of the excitation rate reduction alone, we set $r = r_0$ and $A = A_0$. Other parameter values are given in Table 1.

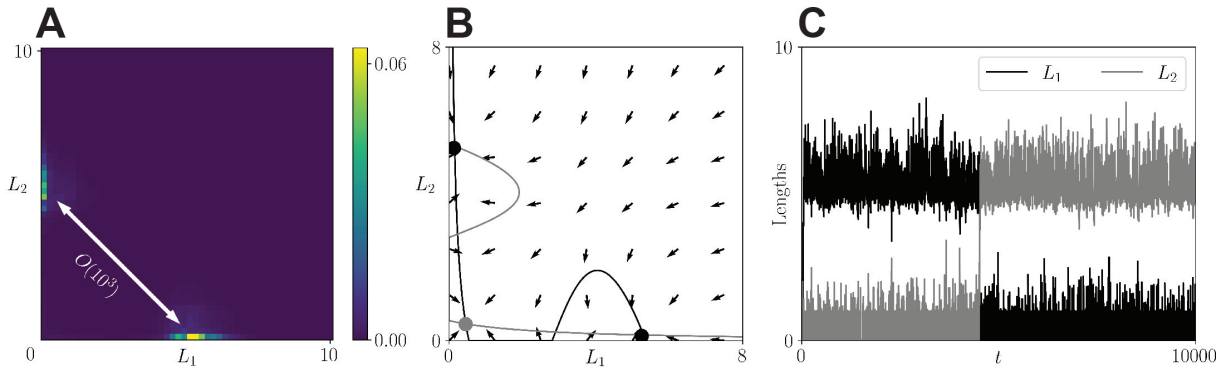


Figure 5: The dynamics of the two-neurite system with negative feedback implemented through both a length-dependent increase in the retraction rate and a decrease in the excitation rate. (A) The long-term probability density is bimodal with two polarized states. The mean transition time between these states is $O(10^3)$. (B) The phase portrait shows two stable polarized equilibria and a stable equilibrium with small basin of attraction in which both neurites are short. (C) A Monte Carlo simulation shows the system flipping between the two polarized states. We set $\alpha = 0.02$ and $A = A_0$ here. Other parameter values are given in Table 1.

151 Metastability Resulting from Different Forms of Negative Feedback

152 We demonstrated above that regardless of the target of the negative feedback, the system enters a polarized state for
 153 some time before exiting to either (1) a different polarized state (i.e., flipping) or (2) a nonpolarized state (i.e., a state
 154 in which both neurites are long). However, the time that the system is in the polarized state varies greatly with the
 155 different forms of negative feedback. In this section, we examine why the persistence of the metastable polarized state
 156 is so different with the different negative feedback mechanisms. For this, we employ a tool called the ϵ -committor,
 157 developed by Lindner et al. [29]. It provides an estimate of the probability that a stochastic trajectory remains in a
 158 region of phase space for a duration of $1/\epsilon$, where ϵ is the rate at which the trajectory is moved into an absorbing state
 159 connected to the region. A definition and description of the calculation of the ϵ -committor is given in the Appendix.

160 We focus on a region that encloses the upper left peak in any of the bimodal probability densities in the previous
 161 section: $R_S = [0, L_b] \times [L_b, L_{\max}]$ in the phase space (see Appendix for the definition of L_{\max}). By definition, the
 162 ϵ -committor corresponding to R_S characterizes the persistence of the polarized state in which $L_2 \gg L_1$, for any of
 163 the three negative feedback mechanisms. Denote this ϵ -committor by C_ϵ . For each form of negative feedback, we
 164 calculate C_ϵ at different values of ϵ . Figure 7A shows that when the negative feedback is on the excitation amplitude,

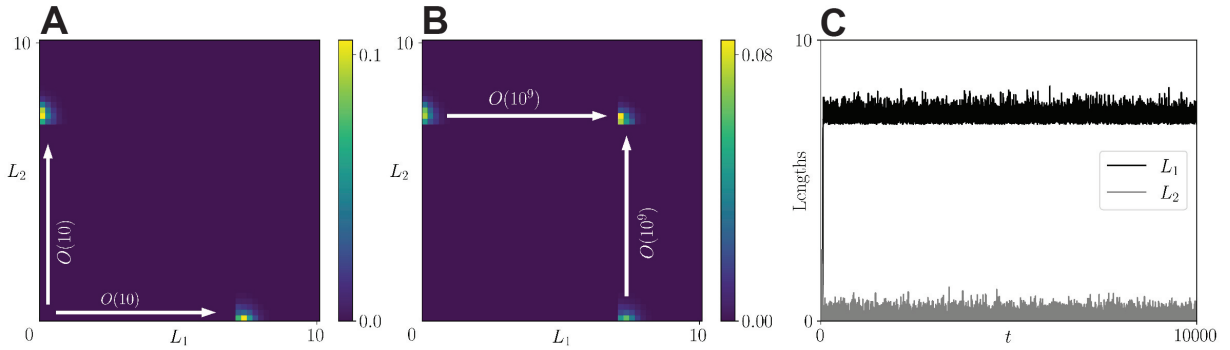


Figure 6: The dynamics of the two-neurite system with negative feedback implemented through a length-dependent decrease in the excitation amplitude. (A) The probability density at $t = 10^6$ is bimodal. (B) The addition of another peak in the probability distribution occurs much later, after $O(10^9)$ time units. (C) A Monte-Carlo simulation shows a persistent polarized state. To study the effect of the excitation amplitude reduction alone, we set $r = r_0$ and $\lambda = \lambda_0$. Other parameter values are given in Table 1.

165 $C_\epsilon \approx 1$ over a timescale of 10^8 , meaning that with high probability a trajectory starting in R_S remains in R_S during
166 this period of time. In contrast, C_ϵ falls to zero much earlier when the negative feedback is on the excitation rate.
167 This indicates that the system leaves R_S quickly and explains the rapid transition from a bimodal probability density
168 to a unimodal probability density corresponding to two long neurites (Fig. 4). C_ϵ starts to drop even earlier when
169 the negative feedback is on the retraction rate, and it reaches ≈ 0.4 . This means that the system spends about 40%
170 of time in R_S in the long run, consistent with its flipping behavior. These ϵ -committor results demonstrate again
171 that applying the length-dependent negative feedback to the excitation amplitude works best in maintaining a unique
172 polarized state.

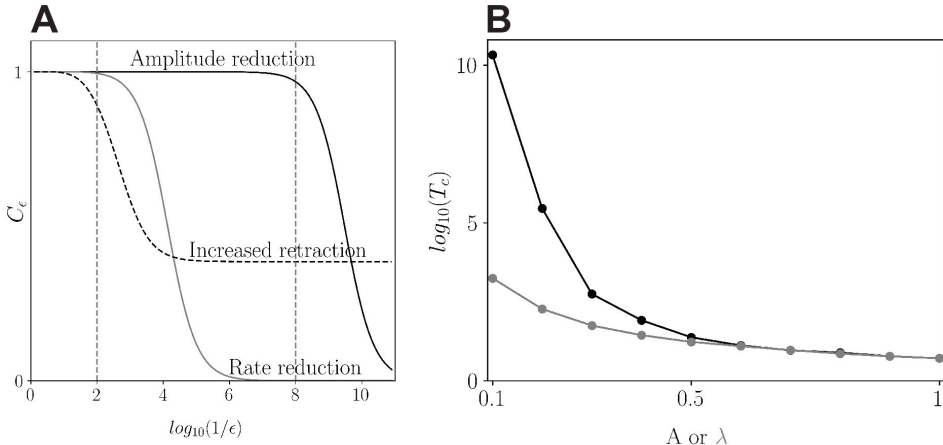


Figure 7: Metastability resulting from different forms of negative feedback. (A) Strength of attraction of the polarized state S is measured by the ϵ -committor C_ϵ . Within the time window marked by the vertical dashed lines, C_ϵ is almost 1 when negative feedback is applied to the excitation amplitude, whereas it drops significantly when applied to the excitation rate or retraction rate. (B) The mean escape time T_c for a single neurite to surpass the threshold L_b increases faster when the excitation amplitude A is reduced (black) than when the excitation rate λ is reduced (grey).

173 The difference in the variations of C_ϵ when negative feedback is on excitation amplitude versus rate can also be
174 quantified via the mean escape time. That is, the time at which a trajectory in a polarized state escapes to the other
175 polarized state or to the nonpolarized state. Consider a single neurite of length L that follows Eq. (1). We use the
176 general cell-mapping method (see Appendix) to calculate the mean time that L , starting at $L = 0$, exceeds L_b for
177 different values of A and λ (mimicking the effects of negative feedback on either of these two targets).

178 We find that the mean escape time (denoted by T_c) increases faster as the excitation amplitude is reduced than
179 when rate is reduced (Fig. 7B). Therefore, reducing the excitation amplitude is more effective than reducing excitation

180 rate on keeping a trajectory within an attracting basin. This explains the long persistence of the polarized state with
 181 negative feedback upon excitation amplitude.

182 Finally, we estimate the probability of crossing the threshold L_b starting from $L = 0$ for a single neurite. To
 183 overcome retraction, the neurite must receive at least L_b/A excitations during a short period (for simplicity, we
 184 assume that L_b/A is an integer here, which is true for the parameter values listed in Table 1. If L_b/A is not an integer,
 185 we need to round it up to the nearest integer. But this won't affect our result qualitatively). Consider $\tau = 1/r$,
 186 the timescale of retraction. Let P_c be the probability of having L_b/A excitations during τ , which follows a Poisson
 187 distribution:

$$P_c = \frac{(\lambda\tau)^{\frac{L_b}{A}} e^{-\lambda\tau}}{\left(\frac{L_b}{A}\right)!}. \quad (6)$$

188 With the Stirling's Approximation for factorial

$$n! = \sqrt{2\pi n} \left(\frac{n}{e}\right)^n, \quad (7)$$

189 we get

$$\ln(P_c) = \frac{L_b}{A} \left[\ln(\lambda\tau) - \ln \frac{L_b}{A} + 1 \right] - \frac{1}{2} \ln \frac{L_b}{A} - \lambda\tau - \frac{1}{2} \ln(2\pi). \quad (8)$$

190 If the amplitude A is reduced to A/m ($m > 1$) and λ remains unchanged, then

$$\ln(P_c) = m \frac{L_b}{A} \left[\ln(\lambda\tau) + 1 - \ln \frac{L_b}{A} - \ln(m) \right] - \frac{1}{2} \ln \frac{L_b}{A} - \frac{1}{2} \ln(m) - \lambda\tau \frac{1}{2} \ln(2\pi). \quad (9)$$

Thus, $\ln(P_c)$ decreases faster than linear reduction. To see this more clearly, we plug in the parameter values in Table 1, namely $L_b = 3$, $A = 1$, $\lambda = 1$, $\tau = 1/r = 1$, and get

$$\begin{aligned} \ln(P_c) &= 3m[1 - \ln(3) - \ln(m)] - \frac{1}{2} \ln(m) - \frac{1}{2} \ln(3) - \frac{1}{2} \ln(2\pi) - 1 \\ &\sim -3m \ln(m), \quad \text{for large } m. \end{aligned} \quad (10)$$

191 On the other hand, if A is unchanged and λ is reduced to λ/m ($m > 1$), then

$$\ln(P_c) = -\frac{L_b}{A} \ln(m) + \frac{L_b}{A} \ln(\lambda\tau) - \frac{\lambda\tau}{m} - \frac{L_b}{A} (\ln \frac{L_b}{A} - 1) - \frac{L_b}{A} - \frac{1}{2} \ln(2\pi). \quad (11)$$

With the parameter values mentioned above, we get

$$\begin{aligned} \ln(P_c) &= -3 \ln(m) - \frac{1}{m} - 3(\ln(3) - 1) - \frac{1}{2} \ln(3) - \frac{1}{2} \ln(2\pi) \\ &\sim -3 \ln(m), \quad \text{for large } m, \end{aligned} \quad (12)$$

192 where we can see that $\ln(P_c)$ decreases with m logarithmically. Thus, the probability of crossing the threshold is
 193 much larger at small excitation rate compared with the probability at a small excitation amplitude. One can conclude
 194 from this that the persistence in a single polarized state is greater when negative feedback is applied to excitation
 195 amplitude.

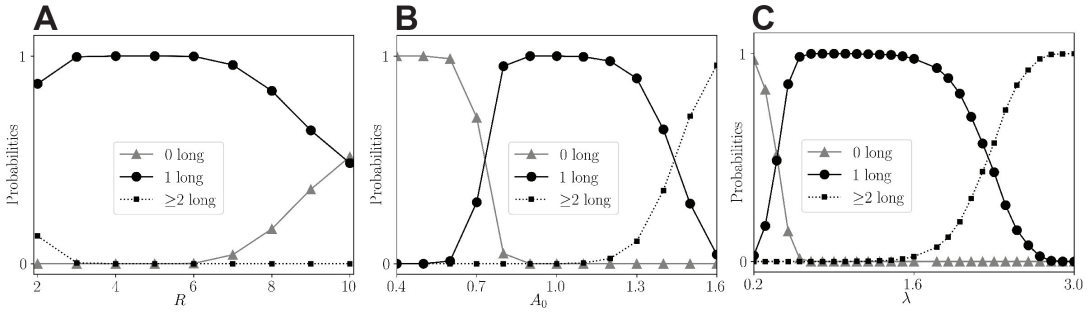


Figure 8: Probabilities of having 0, 1 and ≥ 2 long neurites when the negative feedback is targeted to the excitation amplitude. (A) Varying neurite number R , with $A_0 = \lambda = 1$. (B) Varying base amplitude A_0 , with $R = 4$ and $\lambda = 1$. (C) Varying excitation rate λ , with $R = 4$ and $A_0 = 1$. Each probability is obtained by running 2000 Monte Carlo simulation trials up to time 10000. For all simulations, $\phi = 0.1$ and other parameter values are as in Table 1.

196 Polarization With More Than Two Neurites

197 Most developing neurons have between 2 and 10 neurites [2]. We next focus on the most effective form of negative
 198 feedback, targeted to the excitation amplitude, in model systems with more than 2 neurites. Results are obtained
 199 through Monte Carlo simulations, since the GCM approach to obtaining probability distributions is computationally
 200 expensive at higher dimensions. We seek to determine how the number of neurites R , as well as excitation amplitude
 201 and frequency, impact the probability of obtaining a single persistent polarized state.

202 The first set of results shows that the probability of obtaining a persistent polarized state first rises and then falls
 203 with the number of neurites, and the probability is almost 1 when R is from 3 to 6 (Fig. 8A). Within this range, the
 204 probabilities of having a state with 0 or ≥ 2 long neurites is almost zero. At smaller values of R , the probability of
 205 having ≥ 2 long neurites increases. In this case the actin waves are distributed among a smaller number of neurites,
 206 so that each receives more excitation that can push it across the threshold from short to long. At larger R values
 207 the probability of having no long neurites increases, since each neurite receives fewer actin waves and thus it becomes
 208 more likely that none will go past the threshold.

209 When the number of neurites is held constant at $R = 4$, an optimal range of parameter values exists for either the
 210 basal excitation amplitude or the excitation rate (Fig. 8B and C). If either parameter is too small, then the size or
 211 frequency of actin waves are too small for any of the neurites to cross over from small to long. If either parameter is
 212 too large, then more than one neurite will cross over despite of the negative feedback. The optimum range for all three
 213 parameters, R , A_0 , and λ depend on the values of other parameter, as they are determined by the balance among
 214 excitatory pulses, retraction, and negative feedback. A change in the value of any one parameter changes the balance.

215 Bistability and Excitation Amplitude Reduction in a Limited-Resource 216 Model

217 There have been several modeling studies in which the biophysical mechanism underlying neuronal polarization was
 218 competition for a limited supply of some growth factor or structural protein; the neurite acquiring the most becomes
 219 an axon [14, 16, 21, 30]. In this section, we show how bistability and excitation amplitude reduction are involved in
 220 this mechanism.

To illustrate, we build a simple model based on [16]. Consider a neuron with two neurites whose growth is supported by some growth factor F produced at the cell body. F is transported by actin waves to the neurite tips and diffuses back to the cell body. As in [16], we assume that F slows down the retraction of the neurites. Let C_0 , C_1 and C_2

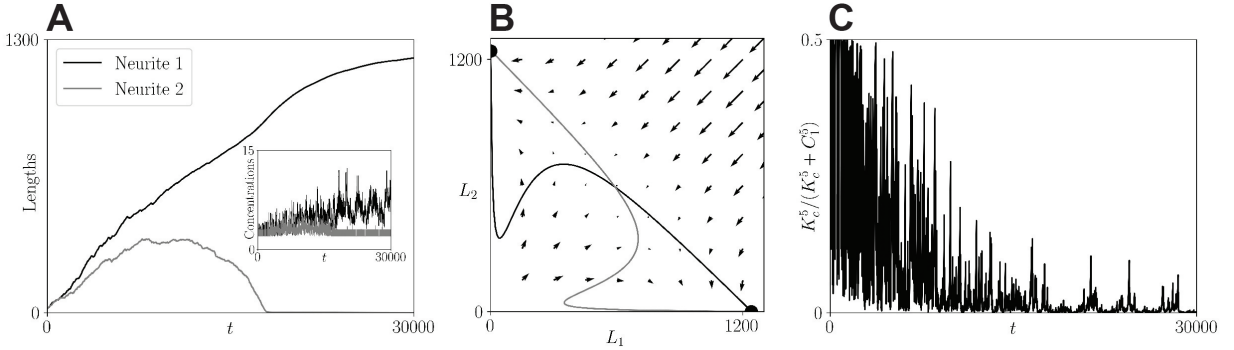


Figure 9: Neuronal polarization with a limited-resource model. (A) A Monte Carlo simulation reproduces the emergence of a single axon. The inset shows the time evolution of the concentrations of the growth factor at two neurite tips. (B) The reduced two-dimensional system shows two stable equilibria (black filled circles). (C) For the neurite that develops into the axon (neurite 1), the fluctuation in its retraction rate, represented by $K_c^5/(K_c^5 + C_1^5)$, becomes smaller as the neurite grows over time. Parameter values for these results are given in Table 2.

be the concentrations of F at the cell body and the neurite tips. These quantities, and neurite lengths L_i , evolve according to:

$$\frac{dC_i}{dt} = -\frac{C_i - C_0}{aL_i} + B \sum_j \delta(t - t_j^{(i)}(\lambda)), \quad (13)$$

$$\frac{dL_i}{dt} = b - r_a(L_1 + L_2) - r_b \frac{K_c^5}{K_c^5 + C_i^5} \frac{L_i}{L_i + G}. \quad (14)$$

The first term on the right-hand side of Eq. (13) describes the Fickian flux of F which is proportional to the concentration gradient $(C_i - C_0)/L_i$. Unlike [16], we assume that C_0 is constant, so that the total amount of F is not conserved. (The results below are similar whether the growth factor is conserved or not.) The second term represents actin waves carrying the growth factor F . The term approximates the narrow Gaussian spikes used in the original model [16]. Each wave causes a jump of size B in concentration. The first two terms of Eq. (14) describe the growth of a neurite that is limited by a common resource that is used up as the neurites become longer (e.g., the protein tubulin, which is a key constituent of microtubules). The third term is the retraction rate that is reduced when growth factor is present. It retains the key properties of the original retraction term in the model in [16]: (1) the sharp reduction in the retraction rate as C_i gets closer to K_c ; (2) the sigmoidal increase of the retraction rate with L_i .

Notation	Definition	Value
a	Diffusion parameter	0.121
B	Excitation amplitude	1*
λ	Excitation rate	0.059
b	Maximum growth rate	0.25
r_a	Fixed retraction rate	0.0002
r_b	Maximum fluctuating retraction rate	0.5
K_c	Half activation level	2
C_0	Concentration at the cell body	2

Table 2: List of parameters in the limited-resource model. We choose a constant excitation amplitude ($B = 1$), reflecting a constant level of growth factor at the cell body ($C_0 = 2$). Other parameter values are as in [16].

Using parameter values based on experimental measurements in [16] (see Table 2), Monte Carlo simulations reproduce the emergence of a single axon (Fig. 9A). Although fluctuating, the factor mostly accumulates in the long neurite that ultimately becomes the axon. To see bistability in the model, we replace the pulse term in Eq. (13) by its average

$B\lambda/2$ to obtain an auxiliary deterministic system:

$$\frac{dC_i}{dt} = -\frac{C_i - C_0}{aL_i} + \frac{B\lambda}{2}, \quad (15)$$

$$\frac{dL_i}{dt} = b - r_a(L_1 + L_2) - r_b \frac{K_c^5}{K_c^5 + C_i^5} \frac{L_i}{L_i + G}. \quad (16)$$

230 This system evolves on two disparate time scales, with the growth factor concentrations changing much more rapidly
 231 than the neurite lengths. In the quasi-steady state, in which $dC_i/dt = 0$, C_i is given by

$$C_i = C_0 + \frac{B\lambda a L_i}{2}. \quad (17)$$

232 Substituting this expression for C_i into Eq. (16), we get a two-dimensional system for L_1 and L_2 , whose phase portrait
 233 is shown in Fig. 9B. The two stable equilibria in the phase plane demonstrate the bistability in the model at the two
 234 polarized states.

235 To see that the model employs length-dependent excitation amplitude reduction, we plot $K_c^5/(K_c^5 + C_i^5)$ for the
 236 neurite that developed into the axon ($i = 1$ for the case shown in Fig. 9A), which provides for random fluctuation in its
 237 retraction rate. As Fig. 9C shows, the fluctuation becomes progressively smaller as the neurite grows. As a result, the
 238 “stochastic noise” in the neurite length is damped as the neurite grows, reflecting an excitation amplitude reduction.
 239 Physically, the decay of the fluctuation results from the decreasing Fickian flux as the neurite grows, which facilitates
 240 growth factor accumulation. Length-dependent Fickian flux was also involved in other limited-resource models [21, 30].

241 In the original model [16], the total amount of the growth factor was assumed to be conserved. Therefore, the
 242 neurites competed for both the growth factor and structural proteins. Also, the excitation amplitude B was assumed
 243 to be proportional to C_0 , which decreased as the neurites grew. This was a second means of reduction in the size of
 244 the stochastic noise. Although unnecessary for successful neuronal polarization, as we showed here, these additional
 245 mechanisms may help the establishment of a single-axon in a noisy biological environment. Redundancy in biological
 246 processes is common in biological systems [24].

247 Discussion

248 In this article, we developed and analyzed a minimal model for achieving neuronal polarization that is based on
 249 what we believe to be the two key ingredients of the polarization process: bistability and length-dependent negative
 250 feedback. The bistability is necessary for the formation of two distinct classes of neurites (short and long), while the
 251 length-dependent negative feedback assures that once a neurite becomes long the others are prohibited from doing so.
 252 While there are several plausible targets of the negative feedback in the minimal model, we demonstrated that one
 253 stands out as the most effective in achieving persistent polarization. The success of this mechanism, targeted to the
 254 amplitude of stochastic actin waves, was demonstrated in several ways, including the joint probability distribution,
 255 Monte Carlo simulations, a large ϵ -committor, a long escape time from a polarized state, and a low escape probability.
 256 Additionally, we found that with this negative feedback mechanism, polarization is more successful if there are more
 257 than two neurites competing in the winner-takes-all contest. Finally, we demonstrated that a neuronal polarization
 258 model based on competition for a limited growth factor has the same underlying key ingredients as our most successful
 259 minimal model: bistability and length-dependent reduction in the excitation magnitude.

260 The clear distinctions between the axon and other short neurites of a neuron during its polarization indicate an
 261 inherent bistability [1, 31]. Typically, bistability arises from positive feedback [24], and various sources of positive

feedback have been identified. One example involves length-dependent retrograde diffusion flux of polarity effectors [4, 16, 21]. Another results from the anterograde transportation of polarity effectors that is enhanced by their accumulation at neurite tips [14], possibly due to stabilization of microtubules [22]. Microtubule stabilization was also shown to help the localization of endoplasmic reticulum tubules, which in turn enhanced the stabilization [23]. Some of the signaling pathways involved in polarization are discussed in [10, 13, 15, 20].

Another major element of positive feedback in neurite growth is the autocrine effects of neurotrophic factors such as Brain-Derived Neurotrophic Factor (BDNF) and neurotrophin-3 (NT-3). These factors are released by individual neurites and bind to receptors on the neurites, stimulating their growth. It has been shown that BDNF activation of its receptor TrkB not only promotes neurite growth, but provides positive feedback by promoting BDNF secretion [19]. The impact of the local neurotrophin secretion depends on the receptor density at the neurite tip, and it has been shown that neurotrophin binding to receptors recruits more receptors to the membrane, thus providing positive feedback in the response to the neurotrophin [19, 32].

Once an axon has formed, negative feedback mechanisms are necessary to prevent the formation of a second axon. In this study, we examined three different unbiased negative feedback mechanisms. Length-dependent increased retraction prevents the growth of a short neurite by destroying its bistability. This negative feedback may result from long-range signals emitted from neurite tips [33], or from a competition for material proteins [16]. We showed that this mechanism is successful in creating polarized states, but does not prevent flipping between the polarized states, which does not appear to occur in actual neurons. This demonstrates that maintenance of a unique polarized state depends on length-dependent suppression of random actin waves, at least in the case of unbiased negative feedback. It is certainly possible that some form of biased negative feedback occurs, in which only a long neurite can initiate the negative feedback. One example of this is with the neurotrophin NT-3. This growth factor can accumulate at a long neurite and initiate Ca^{2+} waves that travel from the neurite tip back to the cell body, activating the small GTPase RhoA that inhibits growth of all neurites [34]. Thus, a growth factor can contribute to neuronal polarization by both facilitating growth of a neurite exposed to it and by inhibiting the growth of competing neurites.

In addition to increased retraction, we also studied the effects of reducing excitation rate and magnitude. We found that reducing excitation rate was insufficient for preventing the formation of a second axon, while reducing excitation magnitude effectively maintained the polarization of our model neuron. It was observed in previous experiments that the frequency of actin waves (i.e., the average number of actin waves per unit time) and the net growth driven by a single actin wave both decreased after an axon had formed [18]. Our study suggests that the decrease in net growth is a more crucial factor in preventing the formation of a second axon.

Previous studies have proposed a mechanism in which all neurites compete for a limited amount of growth proteins, and the neurite that acquired the most becomes an axon [16, 20]. It was assumed that the axon's acquisition of these proteins was facilitated by active anterograde transportation and retrograde diffusion. Using a simplification of one such model [16], we demonstrated that this mechanism exhibits bistability and a length-dependent reduction in excitation magnitude. The excitation magnitude reduction results from the axon's decreased diffusion flux as it grows. Length-dependent diffusion flux is not the only means of preventing the redistribution of growth proteins. It is also possible that blockage occurs in the long neurites. This was demonstrated in a study showing a novel cytoskeletal mechanism in which a dampened retrograde microtubule network assists in the accumulation of Kinesin-1 in the neurite that becomes the axon [35]. Similar to the effect of slow diffusion, the retrograde transportation of Kinesin-1 is reduced, which prevents its redistribution among all neurites.

Our model's bistability and reduction in excitation magnitude may not completely prevent the emergence of multiple axons, which could be considered a flaw. However, a previous experimental study found that a short neurite

304 was able to develop into an axon when it was mechanically stretched, even after another axon had already formed [31].
305 Our model easily explains this result, as mechanical stretching can cause a neurite to surpass the threshold length,
306 putting it into the basin of attraction of the higher stable equilibrium, regardless of whether another axon already
307 exists. In contrast, a limited resource model that does not allow for more than one axon could not account for this
308 experimental finding.

309 In a prior experimental study by Wissner-Gross et al., it was observed that neurons with varying numbers of
310 neurites polarized synchronously [2]. The authors found that prior models based on competition for a limited resource
311 [16, 36] failed to replicate this, but instead the polarization time increased with the number of neurites. However, if the
312 amount of the limited resource was increased with the number of neurites, the polarization time was similar for model
313 cells with different numbers of neurites. Indeed, they found that the levels of two polarity factors, Shootin1 and HRas,
314 were both higher in neurons with more neurites. We find similar behavior with our models. In the minimal model
315 (Eq. (1)), if the basal excitation amplitude A_0 is properly up-regulated according to the neurite number, the time to
316 polarize will be similar regardless of the number of neurites. Similarly, for our limited-resource model (Eqs. (13) and
317 (14)), if the concentration of the growth factor at the cell body, C_0 , is adjusted based on the neurite number, the
318 time to polarize will remain unchanged. The Wissner-Gross study also found that the majority of rat hippocampal
319 neurons grown in cell culture had between 5 and 7 neurites [2], suggesting the existence of an optimal range for the
320 number of neurites, as in our Fig. 8, and raising the possibility of a regulatory mechanisms for achieving polarization
321 by modulating both the number of neurites and the levels of effectors.

322 Acknowledgement

323 We thank Michael Lindner for helpful discussions. BRK would like to thank his parents, Parthasarathy and Usha
324 Karamched, for their love and unending support.

325 Funding

326 This research was partially supported by the National Science Foundation, grant number DMS 1853342, to R. Bertram.

327 CRediT author statement

328 **Fan Bai:** Conceptualization, Methodology, Software, Writing - Original Draft **Richard Bertram:** Conceptualization-
329 Methodology, Writing - Review & Editing, Funding acquisition **Bhargav R. Karamched:** Conceptualization,
330 Methodology, Writing - Review & Editing

331 Declaration of Competing Interest

332 The authors declare that they have no known competing financial interests or personal relationships that could have
333 appeared to influence the work reported in this paper.

334 Appendix

335 The generalized cell-mapping method

336 The generalized cell-mapping method (GCM) is a numerical implementation of the transfer operator (also called the
 337 Perron–Frobenius operator), often used to find the probability distributions of the quantities in a random dynamical
 338 system [37–42]. The GCM is also called Ulam’s method (see [29, 43, 44] and the references therein). The idea of
 339 the GCM is to discretize the system into a discrete-time Markov chain, and to calculate the distribution using the
 340 transition matrix. We use this method to compute probability distributions of neurite length.

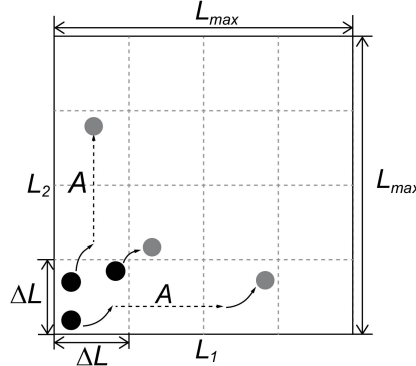


Figure 10: Illustration of the generalized cell mapping method. The phase space of size $L_{\max} \times L_{\max}$ is divided into small square cells of size $\Delta L \times \Delta L$. Starting from a sample point, the two-neurite system may follow a continuous trajectory to reach another cell, or a discontinuous trajectory with a jump of size A in L_1 or L_2 . The black and the grey dots mark the starting and ending positions, respectively. For purposes of illustration, the region is split into 4×4 cells. In actual simulations, we choose $\Delta L = 0.2$ and $L_{\max} = 10$, so that there are 50 cells in each direction. The time increment Δt to generate the trajectories is 0.1.

341 To illustrate the method, consider a system of two neurites. We aim at finding the joint probability distribution
 342 $p(L_1, L_2, t)$ of neurite lengths, L_1 and L_2 , at time t . We consider a region $[0, L_{\max}] \times [0, L_{\max}]$, where the upper bound
 343 L_{\max} is large enough so that $p(L_1, L_2, t)$ is negligible outside the region. Then we divide the region into $N \times N$ square
 344 cells of width ΔL ($\Delta L = L_{\max}/N$), as shown in Fig. 10, and denote the cell in the i th row and j th column as $C_{i,j}$
 345 ($i, j = 1, 2, \dots, N$). To discretize time, we choose a small time increment Δt and only consider the distribution at
 346 $t = n\Delta t$ ($n = 0, 1, \dots$). Then the probability that (L_1, L_2) falls within $C_{i,j}$ at $t = n\Delta t$, denoted by $p_{i,j}(n)$, is given by

$$p_{i,j}(n) = \Pr\{(L_1, L_2) \in C_{i,j} \text{ at } t = n\Delta t\} = \int_{(l_1, l_2) \in C_{i,j}} p(l_1, l_2, t) \, dl_1 dl_2, \quad (18)$$

347 where the notation $(l_1, l_2) \in C_{i,j}$ means that $l_1 \in [(i-1)\Delta L, i\Delta L]$ and $l_2 \in [(j-1)\Delta L, j\Delta L]$.

348 Let

$$\mathbf{p}(n) = (p_{1,1}(n), p_{1,2}(n), \dots, p_{N,N}(n)) \quad (19)$$

349 be an 1-by- N^2 probability vector at time step n . Define the transition probability matrix \mathbf{Q} as

$$\mathbf{Q} = \begin{bmatrix} Q_{(1,1) \rightarrow (1,1)} & Q_{(1,1) \rightarrow (1,2)} & \dots & Q_{(1,1) \rightarrow (N,N)} \\ Q_{(1,2) \rightarrow (1,1)} & Q_{(1,2) \rightarrow (1,2)} & \dots & Q_{(1,2) \rightarrow (N,N)} \\ \vdots & \vdots & \ddots & \vdots \\ Q_{(N,N) \rightarrow (1,1)} & Q_{(N,N) \rightarrow (1,2)} & \dots & Q_{(N,N) \rightarrow (N,N)} \end{bmatrix} \quad (20)$$

350 where $Q_{(i',j') \rightarrow (i,j)}$ is the transition probability from $C_{(i',j')}$ to $C_{(i,j)}$ during Δt . (For our model, the Markov chain is
 351 time-independent, so $Q_{(i',j') \rightarrow (i,j)}$ does not depend on n). The probability vector at time step n is related to that at

352 the previous time step by:

$$\mathbf{p}(n) = \mathbf{p}(n-1)\mathbf{Q}, \quad (21)$$

353 or

$$p_{i,j}(n) = \sum_{i',j'=1,2,\dots,N} Q_{(i',j') \rightarrow (i,j)} p_{i,j}(n-1), \quad i,j = 1,2,\dots,N, \quad n = 1,2,\dots \quad (22)$$

354 To estimate $Q_{(i',j') \rightarrow (i,j)}$, we sample M points uniformly in $C_{(i',j')}$. Starting from each point, we could find a
 355 trajectory by solving Eq. (1) with a Monte Carlo method. Let $M_{i,j}$ be the number of trajectories that end in $C_{i,j}$,
 356 then $M_{i,j}/M$ approximates $Q_{(i',j') \rightarrow (i,j)}$. This should be repeated many times and the average taken. This is a time-
 357 consuming procedure, so we employ the more efficient procedure developed in [45]. Starting from each sample point
 358 (i',j') we solve Eq. (1) without the stochastic term over time Δt :

$$\frac{dL_i}{dt} = g \frac{L_i^2}{L_i^2 + K^2} - rL_i, \quad i = 1, 2. \quad (23)$$

359 Let $M_{i,j}^{(d)}$ be the number of trajectories that end in $C_{i,j}$, then $M_{i,j}^{(d)}/M$ approximates the probability of transition
 360 from $C_{(i',j')}$ to $C_{i,j}$, provided no pulse occurs during Δt . (The superscript “ (d) ” represents “deterministic”.) Then we
 361 consider the case where a single pulse occurs during Δt . Since we describe actin waves as a Poisson process, the time
 362 of the occurrence is uniformly distributed within Δt [46]. Thus, we solve Eq. (23) over $\Delta t/2$, then randomly choose a
 363 length from L_1 and L_2 and add A to it, and finally solving Eq. (23) over the rest of the time interval $\Delta t/2$ (Fig. 10).
 364 The result is a trajectory with a single discontinuity. We repeat the same calculation for all sample points. Let $M_{i,j}^{(s)}$
 365 be the number of trajectories that end in $C_{i,j}$, then $M_{i,j}^{(s)}/M$ approximates the probability of transition from $C_{(i',j')}$
 366 to $C_{i,j}$, provided a single pulse occurs during this short period. (The superscript “ (s) ” represents “stochastic”.) Since
 367 the probability of having two or more pulses during Δt is of $O(\Delta t^2)$, we neglect this probability and approximate
 368 $Q_{(i',j') \rightarrow (i,j)}$ as

$$Q_{(i',j') \rightarrow (i,j)} = (1 - \lambda\Delta t) \frac{M_{i,j}^{(d)}}{M} + \lambda\Delta t \frac{M_{i,j}^{(s)}}{M}, \quad (24)$$

369 where $\lambda\Delta t$ is the first order approximation of the probability of having a single pulse during Δt . In principle, one
 370 could refine the approximation by dividing Δt into more subintervals.

371 Given an initial distribution $\mathbf{p}(0)$, we can calculate $\mathbf{p}(n)$ iteratively with Eq. (21). To obtain $\mathbf{p}(0)$, suppose that
 372 the system starts from $(L_1(0), L_2(0))$. We find the cell $C_{i,j}$ containing this point and set the corresponding $p_{i,j}(0)$ to
 373 be 1 and all other probabilities to be 0. To estimate the limiting distribution $\mathbf{p}(\infty)$, we iterate according to Eq. (21),
 374 until the change in $\mathbf{p}(n)$ becomes negligible. To speed up the iteration, we utilize $\mathbf{Q}^{2^k} = (\mathbf{Q}^{2^{k-1}})^2$, such that $\mathbf{p}(2^k)$
 375 can be obtained with k iterations.

376 In addition to solving the distribution, we will also use the GCM to calculate various first passage probabilities
 377 and mean first passage times. This requires modification of the transition matrix \mathbf{Q} . Suppose we are interested in
 378 finding the probability that the two-neurite system enters a specific region \mathcal{D} and the mean entering time. For a cell
 379 centered within \mathcal{D} , the transition probability $Q_{(i',j') \rightarrow (i,j)}$ is modified as $\tilde{Q}_{(i',j') \rightarrow (i,j)}$:

$$\tilde{Q}_{(i',j') \rightarrow (i,j)} = \begin{cases} 1, & (i,j) = (i',j') \\ 0, & \text{otherwise} \end{cases} \quad (25)$$

380 This makes \mathcal{D} an absorbing region, which means that once the system enters \mathcal{D} , it is frozen and cannot make further
 381 transitions. Let the modified transition matrix be $\tilde{\mathbf{Q}}$ and the resulting distribution be $\tilde{\mathbf{p}}(n)$. The probability of entering

382 \mathcal{D} at $t \leq n\Delta t$ is given by

$$P_{\mathcal{D}}(n) = \sum_{C_{i,j} \in \mathcal{D}} \tilde{p}_{i,j}(n), \quad (26)$$

383 where $C_{i,j} \in \mathcal{D}$ means that the center of $C_{i,j}$ is in \mathcal{D} . The probability of entering \mathcal{D} is given by

$$\Pr\{\text{Entering } \mathcal{D}\} = P_{\mathcal{D}}(\infty) = \sum_{C_{i,j} \in \mathcal{D}} \tilde{p}_{i,j}(\infty), \quad (27)$$

384 which can be obtained by iterating enough number of times according to $\tilde{\mathbf{p}}(n) = \tilde{\mathbf{p}}(n-1)\tilde{\mathbf{Q}}$. Finally, let $\langle T_{\mathcal{D}} \rangle$ be the
385 mean entering time, then

$$\langle T_{\mathcal{D}} \rangle = \sum_{n=1}^{\infty} n\Delta t (P_{\mathcal{D}}(n) - P_{\mathcal{D}}(n-1)). \quad (28)$$

386 Numerically, the series is truncated to drop the terms that make little contribution.

387 The GCM can be implemented regardless of the dimension of a system of interest. The mean escape time shown
388 in Fig. 7B is calculated by applying the GCM to a single neurite. By setting $\mathcal{D} = [L_b, L_{\max}]$, the mean T_c that the
389 neurite length surpasses the threshold L_b is given by Eq. (28).

390 Monte Carlo simulations

391 In addition to the GCM, we also simulate the time evolution of the neurite lengths using a Monte Carlo method. The
392 algorithm that we use is the following:

- 393 (1) Set the initial lengths $L_i(0) = 0$, $(i = 1, 2, \dots, R)$.
- 394 (2) At each time step $t = n\Delta t$, add to each $L_i(t)$ the deterministic increment $\Delta t[gL_i^2/(L_i^2 + K^2) - rL_i]$.
- 395 (3) Generate a random number u within $[0, 1]$. If $u > \lambda\Delta t$, go back to Step (2). Note that λ may be variable if
396 there is length-dependent rate reduction (Eq. (3)).
- 397 (4) If $u \leq \lambda\Delta t$, randomly choose an $L_i(t)$ from the N lengths, and add A to it. Note that A may be variable if there
398 is length-dependent amplitude reduction (Eq. (4)). Then go back to Step (2).
- 399 (5) Repeat Steps (2) to (4) until iterations are completed.

400 We choose $\Delta t = 0.1$ for all simulations. The duration of a simulation depends on the type of negative feedback. Monte
401 Carlo simulation is also applied to the winner-takes-all model (Eqs. (13) and (14)), and the implementation is similar.

402 Implementation of the ϵ -committor method

403 The ϵ -committor was introduced by Lindner et al. [29] as a means of estimating the probability that a stochastic
404 trajectory remains in a region of phase space for a duration of $1/\epsilon$. Here, we describe its implementation within the
405 framework of the GCM.

406 Consider the polarized state where $L_1 \ll L_2$, referred to as S in the following. To study its persistence, we choose a
407 rectangular region $\mathcal{R}_S = [0, L_b] \times [L_b, L_{\max}]$, where L_b is the aforementioned location of the potential barrier and L_{\max}
408 is the user-defined boundary of the phase space in both directions. With the parameter values in Table 1, we have
409 $L_b = 3$. The top-left peak of the bimodal probability density resulting from any of the negative feedback mechanisms
410 described above (see Fig. 3, Fig. 4 and Fig. 6) falls into \mathcal{R}_S . Now we introduce two auxiliary absorbing states Z_1 and
411 Z_2 . When the system is in \mathcal{R}_S , it has a probability ϵ of being absorbed into Z_1 at each time step. When the system
412 is in the rest of the region, it is absorbed into Z_2 at each time step with the same probability (Fig. 11). Let $q_{i,j}$ be
413 the probability of being absorbed into Z_1 when the system starts from (the center of) $C_{i,j}$. The probability vector \mathbf{q}

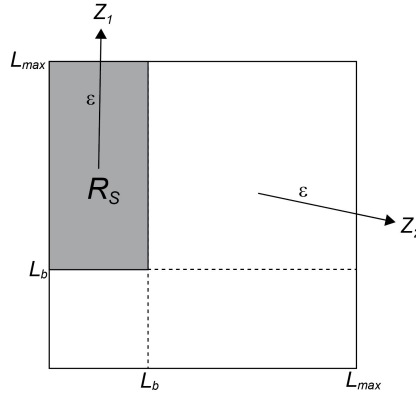


Figure 11: Illustration of the ϵ -committor. Two absorbing states, Z_1 and Z_2 are introduced. When the system wanders within \mathcal{R}_S (grey rectangle covering $[0, L_b] \times [L_b, L_{\max}]$), it has a probability of being absorbed into Z_1 at each time step. If the system is outside \mathcal{R}_S , it has the same probability of being absorbed into Z_2 .

414 formed by all $q_{i,j}$'s is called the ϵ -committor, namely

$$\mathbf{q} = (q_{1,1}, q_{1,2}, \dots, q_{N,N})^T. \quad (29)$$

415 Since the probability of being absorbed at each time step by either Z_1 or Z_2 is ϵ , the mean time till absorption is $\Delta t/\epsilon$,
 416 where Δt is the step size used in the GCM. Over such a timescale, if the system starts from $C_{i,j}$ and spends most of
 417 the time within \mathcal{R}_S , it will have a high probability of being absorbed into Z_1 , i.e., $q_{i,j}$ will be close to 1. Conversely,
 418 if the system never enters \mathcal{R}_S or quickly leaves it without coming back, $q_{i,j}$ will be close to 0 [29]. Therefore, $q_{i,j}$
 419 characterizes the attracting strength of the region \mathcal{R}_S over a timescale of $\Delta t/\epsilon$, when the system starts from $C_{i,j}$. By
 420 choosing a starting cell close to the top left peak of a bimodal distribution and changing the value of ϵ , the resulting $q_{i,j}$
 421 quantifies the persistence of the polarized state S over different timescales under the corresponding negative feedback
 422 mechanism. Specifically, we choose the cell at $[0, 6]$ when the increased retraction is implemented, and the cell at $[0, 7]$
 423 when the excitation rate or amplitude reduction is implemented. The corresponding probability $q_{i,j}(\mathcal{R}_S, \epsilon)$ is denoted
 424 by C_ϵ for notational simplicity.

425 To calculate \mathbf{q} use the formula in [29], given as

$$[\mathbf{I} - (1 - \epsilon)\mathbf{Q}] \mathbf{q} = \epsilon \mathbf{I}_{\mathcal{R}_S}, \quad (30)$$

426 where \mathbf{I} is an N^2 -by- N^2 identity matrix and \mathbf{Q} the transition matrix given by Eq. (20). $\mathbf{I}_{\mathcal{R}_S}$ is an N^2 -by-1 indicator
 427 vector defined as

$$\mathbf{I}_{\mathcal{R}_S} = (\delta_{(1,1),\mathcal{R}_S}, \delta_{(1,2),\mathcal{R}_S}, \dots, \delta_{(N,N),\mathcal{R}_S})^T, \quad (31)$$

428 where

$$\delta_{(i,j),\mathcal{R}_S} = \begin{cases} 1, & (i,j) \in \mathcal{R}_S, \\ 0, & (i,j) \notin \mathcal{R}_S \end{cases}. \quad (32)$$

429 References

430 [1] CG Dotti, CA Sullivan, and GA Bunker. The establishment of polarity by hippocampal neurons in culture.
 431 Journal of Neuroscience, 8(4):1454–1468, 1988.

432 [2] Zachary D. Wissner-Gross, Mark A. Scott, Joseph D. Steinmeyer, and Mehmet Fatih Yanik. Synchronous sym-
 433 metry breaking in neurons with different neurite counts. PLOS ONE, 8(2):1–8, 02 2013.

434 [3] K. Goslin and G. Bunker. Experimental observations on the development of polarity by hippocampal neurons in
435 culture. *J. Cell Biol.*, 108:1507–1516, 1989.

436 [4] Tetsuya Takano, Mengya Wu, Shinichi Nakamuta, Honda Naoki, Naruki Ishizawa, Takashi Namba, Takashi
437 Watanabe, Chundi Xu, Tomonari Hamaguchi, Yoshimitsu Yura, Mutsuki Amano, Klaus M. Hahn, and Kozo
438 Kaibuchi. Discovery of long-range inhibitory signaling to ensure single axon formation. *Nature Communications*,
439 8(1):33, Jun 2017.

440 [5] H. Yamamoto, T. Demura, M. Morita, G. A. Bunker, T. Tanli, and S. Nakamura. Differential neurite outgrowth
441 is required for axon specification by cultured hippocampal neurons. *J. Neurochem.*, 123:904–910, 2012.

442 [6] H. Tabata and K. Nakajima. Multipolar migration: the third mode of radial neuronal migration in the developing
443 cerebral cortex. *J. Neurosci.*, 23:9996–10001, 2003.

444 [7] S. C. Noctor, V. Martinez-Cereno, I. Ivic, and A. R. Kriegstein. Cortical neurons arise in symmetric and asym-
445 metric division zones and migrate through specific phases. *Nat. Neurosci.*, 7:136–144, 2004.

446 [8] N. Inagaki, M. Toriyama, and Y. Sakumura. Systems biology of symmetry breaking during neuronal polarity
447 formation. *Develop. Neurobiol.*, 71:584–593, 2011.

448 [9] G. Bunker. The development of neuronal polarity: a retrospective view. *J. Neurosci.*, 38:1867–1873, 2018.

449 [10] Tetsuya Takano, Yasuhiro Funahashi, and Kozo Kaibuchi. Neuronal polarity: Positive and negative feedback
450 signals. *Frontiers in Cell and Developmental Biology*, 7:69, 2019.

451 [11] N. Arimura and K. Kaibuchi. Neuronal polarity: from extracellular signals to intracellular mechanisms. *Nat.*
452 *Rev. Neurosci.*, 8:194–205, 2007.

453 [12] Amy M Winans, Sean R Collins, and Tobias Meyer. Waves of actin and microtubule polymerization drive
454 microtubule-based transport and neurite growth before single axon formation. *eLife*, 5:e12387, feb 2016.

455 [13] Shaul Yogev and Kang Shen. Establishing neuronal polarity with environmental and intrinsic mechanisms.
456 *Neuron*, 96(3):638–650, 2017.

457 [14] Marc Fivaz, Samuel Bandara, Takanari Inoue, and Tobias Meyer. Robust neuronal symmetry breaking by ras-
458 triggered local positive feedback. *Current Biology*, 18(1):44–50, 2008.

459 [15] Takashi Namba, Yasuhiro Funahashi, Shinichi Nakamuta, Chundi Xu, Tetsuya Takano, and Kozo Kaibuchi.
460 Extracellular and intracellular signaling for neuronal polarity. *Physiological Reviews*, 95(3):995–1024, 2015. PMID:
461 26133936.

462 [16] Michinori Toriyama, Yuichi Sakumura, Tadayuki Shimada, Shin Ishii, and Naoyuki Inagaki. A diffusion-based
463 neurite length-sensing mechanism involved in neuronal symmetry breaking. *Molecular Systems Biology*, 6(1):394,
464 2010.

465 [17] Naoyuki Inagaki and Hiroko Katsuno. Actin waves: Origin of cell polarization and migration? *Trends in Cell*
466 *Biology*, 27(7):515–526, 2017.

467 [18] Gordon Ruthel and Gary Bunker. Role of moving growth cone-like “wave” structures in the outgrowth of cultured
468 hippocampal axons and dendrites. *Journal of Neurobiology*, 39(1):97–106, 1999.

469 [19] P.-L. Cheng, A.-H. Song, Y.-H. Wong, S. Wang, X. Zhang, and M.-M. Poo. Self-amplifying autocrine actions of
470 BDNF in axon development. *Proc. Nat. Acad. Sci.*, 108:18430–18435, 2011.

471 [20] Max Schelski and Frank Bradke. Neuronal polarization: From spatiotemporal signaling to cytoskeletal dynamics.
472 *Molecular and Cellular Neuroscience*, 84:11–28, 2017. Cytoskeleton-dependent regulation of neuronal network
473 formation.

474 [21] Honda Naoki, Shinichi Nakamuta, Kozo Kaibuchi, and Shin Ishii. Flexible search for single-axon morphology
475 during neuronal spontaneous polarization. *PLOS ONE*, 6(4):1–9, 04 2011.

476 [22] Susana Gomis-Rüth, Corette J. Wierenga, and Frank Bradke. Plasticity of polarization: Changing dendrites into
477 axons in neurons integrated in neuronal circuits. *Current Biology*, 18(13):992–1000, 2008.

478 [23] Ginny G. Fariás, Amélie Fréal, Elena Tortosa, Riccardo Stucchi, Xingxiu Pan, Sybren Portegies, Lena Will,
479 Maarten Altelaar, and Casper C. Hoogenraad. Feedback-driven mechanisms between microtubules and the en-
480 doplasmic reticulum instruct neuronal polarity. *Neuron*, 102(1):184–201.e8, 2019.

481 [24] Uri Alon. *An introduction to systems biology*. Taylor & Francis Group, 2020.

482 [25] A. M. Winans, S. R. Collins, and T. Meyer. Waves of actin and microtubule polymerization drive microtubule-
483 based transport and neurite growth before single axon formation. *eLIFE*, 5:e12387, 2016.

484 [26] Naoyuki Inagaki and Hiroko Katsuno. Actin waves: Origin of cell polarization and migration? *Trends Cell Biol.*,
485 27:515–526, 2017.

486 [27] Gordon Ruthel and Gary Bunker. Role of moving growth cone-like “wave” structures in the outgrowth of cultured
487 hippocampal axons and dendrites. *J. Neurobiol.*, 39:97–106, 1999.

488 [28] Honda Naoki and Shin Ishii. Chapter six - mathematical modeling of neuronal polarization during development.
489 In Kim T. Blackwell, editor, *Computational Neuroscience*, volume 123 of *Progress in Molecular Biology and*
490 *Translational Science*, pages 127–141. Academic Press, 2014.

491 [29] Michael Lindner and Frank Hellmann. Stochastic basins of attraction and generalized committor functions. *Phys.*
492 *Rev. E*, 100:022124, Aug 2019.

493 [30] H.G.E. Hentschel, D. Samuels, and A. Fine. Instabilities during the dendritic and axonal development of neuronal
494 form. *Physica A: Statistical Mechanics and its Applications*, 254(1):46–61, 1998.

495 [31] Phillip Lamoureux, Gordon Ruthel, Robert E. Buxbaum, and Steven R. Heidemann. Mechanical tension can
496 specify axonal fate in hippocampal neurons . *Journal of Cell Biology*, 159(3):499–508, 11 2002.

497 [32] C. E. Adler, R. D. Fetter, and C. I. Bargmann. UNC-6/Netrin induces neuronal asymmetry and defines the site
498 of axon formation. *Nat. Neurosci.*, 9:511–518, 2006.

499 [33] Eric R Kandel, James H Schwartz, Thomas M Jessell, Steven A Siegelbaum, and A J Hudspeth, editors. *Principles*
500 *of neural science*. McGraw-Hill, 2013.

501 [34] Tetsuya Takano, Mengya Wu, Shinichi Nakamuta, Honda Naoki, Naruki Ishizawa, Takashi Namba, Takashi
502 Watanabe, Chundi Xu, Tomonari Hamaguchi, Yoshimitsu Yura, Mutsuki Amano, Klaus M. Hahn, and Kozo
503 Kaibuchi. Discovery of long-range inhibitory signaling to ensure single axon formation. *Nat. Comm.*, 8:33, 2017.

504 [35] Mithila Burute, Klara I. Jansen, Marko Mihajlovic, Tina Vermonden, and Lukas C. Kapitein. Local changes
 505 in microtubule network mobility instruct neuronal polarization and axon specification. *Science Advances*,
 506 8(44):eabo2343, 2022.

507 [36] David C. Samuels, H. G. E. Hentschel, and Alan Fine. The origin of neuronal polarization: a model of axon for-
 508 mation. *Philosophical Transactions of the Royal Society of London. Series B: Biological Sciences*, 351(1344):1147–
 509 1156, 1996.

510 [37] J.-Q. Sun and C.S. Hsu. First-passage time probability of non-linear stochastic systems by generalized cell
 511 mapping method. *Journal of Sound and Vibration*, 124(2):233–248, 1988.

512 [38] Y. Wu and W. Q. Zhu. Stochastic analysis of a pulse-type prey-predator model. *Phys. Rev. E*, 77:041911, Apr
 513 2008.

514 [39] Xiaole Yue, Wei Xu, Liang Wang, and Bingchang Zhou. Transient and steady-state responses in a self-sustained
 515 oscillator with harmonic and bounded noise excitations. *Probabilistic Engineering Mechanics*, 30:70–76, 2012.

516 [40] Xiaole Yue, Wei Xu, Wantao Jia, and Liang Wang. Stochastic response of a ϕ 6 oscillator subjected to combined
 517 harmonic and poisson white noise excitations. *Physica A: Statistical Mechanics and its Applications*, 392(14):2988–
 518 2998, 2013.

519 [41] Xiaole Yue, Wei Xu, Yong Xu, and Jian-Qiao Sun. Non-stationary response of mdof dynamical systems under
 520 combined gaussian and poisson white noises by the generalized cell mapping method. *Probabilistic Engineering*
 521 *Mechanics*, 55:102–108, 2019.

522 [42] Qun Han, Wei Xu, Xiaole Yue, and Ying Zhang. First-passage time statistics in a bistable system subject to
 523 poisson white noise by the generalized cell mapping method. *Communications in Nonlinear Science and Numerical*
 524 *Simulation*, 23(1):220–228, 2015.

525 [43] Gary Froyland. *Extracting Dynamical Behavior via Markov Models*, pages 281–321. Birkhäuser Boston, Boston,
 526 MA, 2001.

527 [44] Gary Froyland and Kathrin Padberg. Almost-invariant sets and invariant manifolds — connecting probabilistic
 528 and geometric descriptions of coherent structures in flows. *Physica D: Nonlinear Phenomena*, 238(16):1507–1523,
 529 2009.

530 [45] Hasan Uğur Köylüoğlu, Søren R. K. Nielsen, and Radosław Iwankiewicz. Response and reliability of poisson-driven
 531 systems by path integration. *Journal of Engineering Mechanics*, 121(1):117–130, 1995.

532 [46] Howard M Taylor and Samuel Karlin. *An introduction to stochastic modeling*. Academic press, 2010.